International Journal of Automotive Technology, Vol. ?, No. ?, pp. ?–?(year)

NONLINEAR MODEL PREDICTIVE CONTROL FOR PATH TRACKING IN HIGH-SPEED CORNER ENTRY SITUATIONS

Jonghyup Lee[1], and Seibum Choi[1)*]

[1)] Mechanical Engineering, KAIST, Daejeon 34141, Korea

(*Received date ; Revised date ; Accepted date*) * Please leave blank

ABSTRACT– Path tracking control is one of the essential controls for lateral positioning controls such as collision avoidance and lane keeping and changing. In severe situations in which the tire force reaches its limit, such as entering a corner at high speed or in a low-friction situation, not only accurate path tracking but also stable driving must be ensured. In this paper, an integrated braking and steering controller for path tracking is proposed in consideration of the road friction limit. In particular, individual tire forces were predicted using the vehicle and the tire models, and the results were directly compared with the road friction. A nonlinear model predictive controller (NMPC) was utilized for constrained optimal control using nonlinear models. The proposed controller is verified through vehicle simulators Carsim and MATLAB Simulink. Results show the effectiveness of the proposed controller: it guarantees stable driving and accurate tracking performance.

KEY WORDS : Path tracking control, Nonlinear model predictive control, Tire forces, Road friction limit, Intelligent vehicle, Sequential quadratic programming

NOMENCLATURE

$\boldsymbol{v_x}$: longitudinal velocity, m/s
$\boldsymbol{v_y}$: lateral velocity, m/s
$\boldsymbol{\beta}$: side slip angle, rad
$\boldsymbol{\dot{\psi}}$: yawrate, rad/s
$\boldsymbol{s}$: station, m
$\boldsymbol{e_y}$: lateral offset error, m
$\boldsymbol{e_\psi}$: heading angle error, rad
$\boldsymbol{m}$: vehicle mass, kg
$\boldsymbol{I_z}$: vehicle moment of yaw inertia, kg·m^2
$\boldsymbol{l_f}$: distance from the vehicle's center of mass to front axle, m
$\boldsymbol{l_r}$: distance from the vehicle's center of mass to rear axle, m
$\boldsymbol{w}$: half of the vehicle width, m
$\boldsymbol{\delta}$: wheel steer angle, rad
$\boldsymbol{a_x}$: longitudinal acceleration, m/s^2
$\boldsymbol{a_y}$: lateral acceleration, m/s^2
$\boldsymbol{F_{x,i}}$: longitudinal force of each tire, N
$\boldsymbol{F_{y,i}}$: lateral force of each tire, N
$\boldsymbol{F_{z,i}}$: vertical force of each tire, N
$\boldsymbol{\kappa}$: curvature of the desired path, 1/m
$\boldsymbol{F_D}$: air drag force, N
$\boldsymbol{\lambda}$: brake force ratio of front axle, -
$\boldsymbol{\mu}$: road friction coefficient, -
$\boldsymbol{C_0}$: linear cornering stiffness, N/rad
$\boldsymbol{g}$: gravitational acceleration, m/s^2
$\boldsymbol{h_{cg}}$: height of the vehicle center of mass, m
$\boldsymbol{k_{\varphi f}}$: front roll stiffness, N·m/rad
$\boldsymbol{k_{\varphi r}}$: rear roll stiffness, N·m/rad
$\boldsymbol{h_{rc}}$: distance from roll center to the vehicle's center of mass, m
$\boldsymbol{T_s}$: control period, s
N: the number of step of prediction horizon, -

* *Corresponding author*. e-mail: sbchoi@kaist.ac.kr

1. INTRODUCTION

In recent years, as the importance of vehicle safety has increased, the demand for safety systems is increasing. Advances in sensing technology for intelligent transportation systems have enabled active safety control of vehicles such as autonomous emergency brake, lane change warning system and lane keeping assist system (Wang et al., 2019; Geronimo et al., 2009; Gietelink et al., 2006; Hwang and Choi, 2018). Path tracking control is one of the essential controls for active safety control. The primary task of path tracking control is to follow the planned path stably and accurately(Hu et al., 2018; Lim et al., 2018; Pozna et al., 2009). Therefore, the path tracking controller must prevent unstable movement of the vehicle and minimize lateral offset and heading angle error for the desired path.

Serial#Given by KSAE

Over the past decade, numerous path tracking controllers have been proposed. Existing controllers include the Proportional-Integral-Derivative(PID) controller (Zakaria et al., 2014), H infinity(H_∞) controller(Park et al., 2018; Rigatos and Siano, 2014), sliding mode controller and model predictive controller(MPC) (Liu et al., 2018; Ji et al., 2016). Among these, the MPC generates an optimal control input while considering the constraints on the states and inputs through prediction of future behavior(Xu and Peng, 2019; Paden et al., 2016; Han et al., 2020). It is suitable for path tracking control, which requires accurate and safe control performance, and therefore MPC has been utilized in many path tracking control studies. Path tracking control studies using MPC are designed to satisfy constraints on lateral position, yaw rate or steering angle while minimizing the objective function expressed as a quadratic function. In addition, to consider the nonlinearity of the vehicle model, a study using a nonlinear model predictive controller (NMPC) has been introduced(Wurts et al., 2020; Liu et al., 2018) and, in some cases, linear MPC using a linearized model has been introduced(Simon et al., 2013).

Many existing path tracking studies have used only steering control for path tracking control. These controllers show excellent path tracking performance in smooth driving situations. However, it is difficult to ensure stable vehicle behavior in severe situations such as high-speed or low-friction road conditions. In these situations, due to road friction limitations, the tire does not generate the required lateral force from the controller. As a result, unsafe behavior such as understeer of vehicle occurs. To cope with these situations, the vehicle must be decelerated in advance through appropriate braking control as well as accurate steering control.

For stable path tracking in high-speed situations, combined braking and steering controllers have also been studied (Ren et al., 2020). The simplest existing method assumes the vehicle as a point mass and generates the desired longitudinal speed so that the sum of longitudinal and lateral accelerations does not exceed the road surface limit (Gao et al., 2010). In addition, a controller was proposed to analyze the critical speed limit in steady state cornering and ensure that the vehicle speed is below the limit speed (Siampis et al., 2017). One study conducted speed and steering control through NMPC under the constraint that the vehicle should not roll over (Liu et al., 2017). Unlike studies that proposed a speed limit based on the stability condition, a method that indirectly checks whether the force of each wheel tire does not exceed the road friction limit for the speed and steering input, generated based on the distance from the ego vehicle, has also been proposed (Sazgar et al., 2019). All of these methods enable stabler control than methods that control only in the lateral direction.

However, there are limitations in the stability indicators such as vehicle acceleration or vehicle side slip angle considered in previous studies. Even when these stability indicators are satisfied, if even one tire is saturated during driving, the vehicle's behavior can become rapidly unstable. Therefore, the relatively macroscopic stability indicators of existing studies help to improve vehicle stability, but do not guarantee stability in all situations. Even if these indicators are utilized, it is possible to set an overly restrictive threshold to ensure stable behavior in most situations. However, since the vehicle's behavior is excessively restricted, the range of situations the vehicle can handle is reduced, for example by increasing the braking distance or reducing the type of road surface that can be coped with. Also, increasing the braking distance causes the disadvantage that a larger preview distance is required. Therefore, there is a need for tire force-based indicators that most directly represent vehicle stability. In other words, by utilizing the direct constraint that each tire force not exceed road friction, stable and more active path tracking control is possible.

In this study, we propose an NPMC-based steering and braking controller that consider the limits of each tire force. We used the planar vehicle model and the brushed tire model to predict the tire force for each wheel over the prediction horizon. Through constrained non-linear optimization, control inputs are generated so that the sum of the longitudinal and lateral forces of each tire does not exceed the road friction limit. Sequential quadratic programming (SQP) is used to solve the NMPC problem of the proposed algorithm(Gill and Wong, 2012; Zhu et al., 2016). Through this, the proposed controller automatically generates the optimal amount of braking for stable driving in consideration of the road friction limit. At the same time, it generates an optimal lateral control input to accurately follow the desired path. In this study, it is assumed that the road friction limit is known through various existing road friction estimation algorithms (Khaleghian et al., 2017; Han et al., 2016; Han et al., 2017; Ray, 1997).

The rest of this paper is organized as follows. Section 2 establishes the nonlinear vehicle model including vehicle motions and individual tire forces. Section 3 proposes an NMPC-based path tracking controller considering the road friction limit of each tire. Section 4 validates the path tracking performance of the proposed controller through simulation analysis. Section 5 presents the conclusion.

2. SYSTEM MODELLING

Vehicle motions and individual tire forces are predicted through planar vehicle models and tire models, respectively. The longitudinal, lateral, and yaw motions

Serial#Given by KSAE

of the vehicle on the yaw plane shown in Figure 1 are expressed as follows(Doumiati et al., 2010):

$$\dot{v}_x = \frac{1}{m}\left[\left(F_{x,fl}+F_{x,fr}\right)\cos\delta + F_{x,rl} + F_{x,rr} - \left(F_{y,fl}+F_{y,fr}\right)\sin\delta - F_D\right] + v_x\beta\dot{\psi} \quad (1)$$

$$\dot{\beta} = \frac{1}{mv_x}\left[\left(F_{x,fl}+F_{x,fr}\right)\sin\delta + \left(F_{y,fl}+F_{y,fr}\right)\cos\delta + F_{y,rl} + F_{y,rr}\right] - \dot{\psi} \quad (2)$$

$$I_z\ddot{\psi} = l_f\left[\left(F_{y,fl}+F_{y,fr}\right)\cos(\delta) + \left(F_{x,fl}+F_{x,fr}\right)\sin(\delta)\right] - l_r\left(F_{y,rl}+F_{y,rr}\right) + w(F_{y,fl}\sin\delta - F_{x,fl}\cos\delta - F_{x,rl}) + w(F_{x,fr}\cos\delta - F_{y,fr}\sin\delta + F_{x,rr}) \quad (3)$$

where v_x, β, $\dot{\psi}$, m, I_z, l_f, l_r, w, δ, F_x, F_y and F_D are longitudinal velocity, side slip angle, yawrate, vehicle mass, vehicle moment of yaw inertia, distance from vehicle center of mass to front axle, distance from vehicle center of mass to rear axle, half of vehicle width, wheel steering angle, longitudinal tire force, lateral tire force, and air drag force, respectively. In the planar vehicle model, it is assumed that only the front wheels are steered, and the steering angles of the left and right wheels of the front axle are the same.

It is assumed that the moment inertia of the wheels is negligible and left and right brake pressures are equally applied. It is also assumed that the left and right brake forces are equal(Gray et al., 2012). Then, the longitudinal forces of each wheel are distributed with a constant front-to-rear ratio λ and expressed as:

$$F_{x,fl} = F_{x,fr} = \frac{\lambda}{2}\left[ma_x + \left(F_{y,fl}+F_{y,fr}\right)\delta + F_D\right] \quad (4)$$

$$F_{x,rl} = F_{x,rr} = \frac{(1-\lambda)}{2}\left[ma_x + \left(F_{y,fl}+F_{y,fr}\right)\delta + F_D\right] \quad (5)$$

The lateral tire forces are modeled through a brushed tire model that expresses the nonlinearity of the tire in the high slip region (Svendenius et al., 2009).

$$F_{y,i=}\begin{cases} C_0 tan(\alpha_i) - \frac{C_0^2}{3\mu F_{z,i}}|tan(\alpha_i)|\,tan(\alpha_i)\ldots \\ \quad + \frac{C_0^3}{27\mu^2 F_{z,i}^2}tan^3(\alpha_i), \quad |\alpha_i| < tan^{-1}\left(\frac{3\mu F_{z,i}}{C_0}\right) \\ \mu F_{z,i}\,sgn(\alpha_i), \quad |\alpha_i| > tan^{-1}\left(\frac{3\mu F_{z,i}}{C_0}\right) \end{cases} \quad (6)$$
$$i = fl,\ fr,\ rl,\ rr$$

where C_0 is linear cornering stiffness and μ is the road friction coefficient. The tire slip angles α that generate tire forces are defined as follows, and are approximated due to the relatively large longitudinal velocity.

$$\alpha_{fl} = \alpha_{fr} = tan^{-1}\left(\frac{v_y + l_f r}{v_x}\right) \cong \beta + \frac{l_f}{v_x}\dot{\psi} - \delta \quad (7)$$

$$\alpha_{rl} = \alpha_{rr} = tan^{-1}\left(\frac{v_y - l_r r}{v_x}\right) \cong \beta - \frac{l_r}{v_x}\dot{\psi} \quad (8)$$

where v_y is lateral velocity of vehicle.

The vertical forces on each wheel change due to the load transfer and are expressed as:

$$\begin{cases} F_{z,fl} = \frac{l_r}{2(l_f+l_r)}mg - \frac{h_{cg}}{2(l_f+l_r)}ma_x + \sigma_f ma_y \\ F_{z,fr} = \frac{l_r}{2(l_f+l_r)}mg - \frac{h_{cg}}{2(l_f+l_r)}ma_x - \sigma_f ma_y \\ F_{z,rl} = \frac{l_f}{2(l_f+l_r)}mg + \frac{h_{cg}}{2(l_f+l_r)}ma_x + \sigma_r ma_y \\ F_{z,rr} = \frac{l_f}{2(l_f+l_r)}mg + \frac{h_{cg}}{2(l_f+l_r)}ma_x - \sigma_r ma_y \end{cases} \quad (9)$$

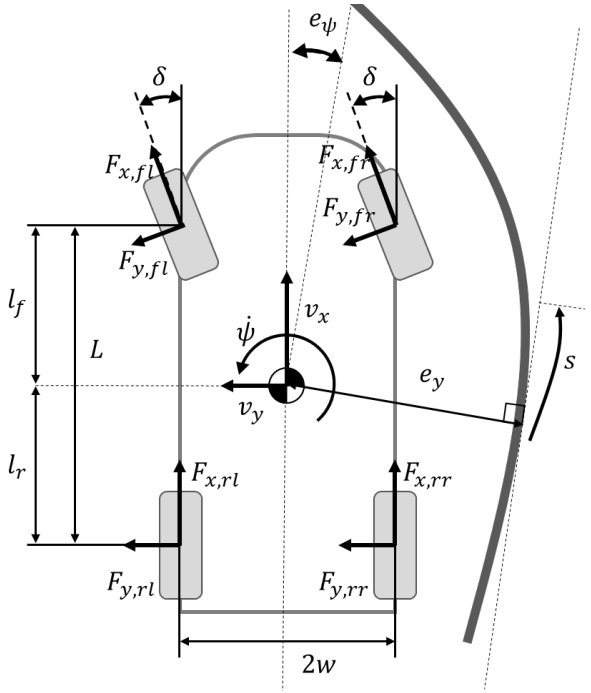

Figure 1. Planar vehicle model and relative positions to desired path

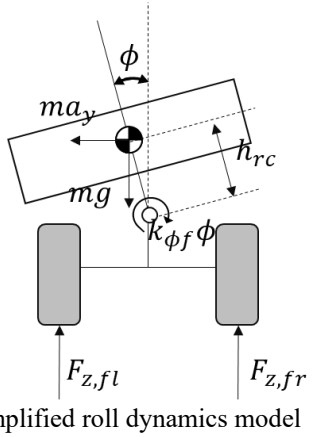

Figure 2. Simplified roll dynamics model

where a_y, h_{cg} and g are lateral acceleration, height of vehicle center of mass and gravitational acceleration. The lateral load transfer coefficients σ_f and σ_r are defined from the vehicle roll motion as follows(Ray, 1997):

$$\begin{cases} \sigma_f = \frac{1}{w}\left(\frac{k_{\varphi f} h_{rc}}{k_{\varphi f} + k_{\varphi r} - mgh_{rc}} + \frac{l_r}{L}\left(h_{cg} - h_{rc}\right)\right) \\ \sigma_r = \frac{1}{w}\left(\frac{k_{\varphi r} h_{rc}}{k_{\varphi f} + k_{\varphi r} - mgh_{rc}} + \frac{l_f}{L}\left(h_{cg} - h_{rc}\right)\right). \end{cases} \quad (10)$$

where $k_{\varphi f}$, $k_{\varphi r}$ and h_{rc} are front and rear roll stiffness and distance between vehicle roll center and vehicle center of mass.

The lateral positional relationship between the desired path and the vehicle is expressed as lateral offset error e_y and heading angle error e_ψ, as shown in Figure 1. Also, station s means the longitudinal vehicle position on the desired path. The dynamic equations of these three states defining the position of the vehicle with respect to the desired path are expressed as follows(Hu et al., 2015):

$$\dot{s} = \frac{1}{1 - \kappa e_y} v_x\left(\cos\left(e_\psi\right) - \beta \sin\left(e_\psi\right)\right) \quad (11)$$

$$\dot{e_y} = v_x\left(\sin\left(e_\psi\right) + \beta \cos\left(e_\psi\right)\right) \quad (12)$$

$$\dot{e_\psi} = \dot{\psi} - \kappa \dot{s} \quad (13)$$

where κ is curvature of desired path.

Finally, we define a control-oriented model usable in the controller. Combining all equations (1)-(13), this model is expressed as follows:

$$\dot{x} = f_c(x(t), u(t)). \quad (14)$$

State vector in (14) is $x = \left[v_x,\ \beta,\ \dot{\psi},\ s,\ e_y,\ e_\psi\right]^T$ and the input vector is $u = \left[a_x,\ \delta_f\right]^T$. To formulate the discrete time MPC framework, the model defined in (14) is discretized using Euler's method with control period T_s, as:

$$x(k+1) = f_d\left(x(k), u(k)\right) = x(k) + f_c\left(x(k), u(k)\right)T_s. \quad (15)$$

3. NMPC DESIGN FOR ACCURATE PATH TRACKING AND STABLE VEHICLE BEHAVIOR

The control inputs of the NMPC used in this study are expressed as solutions of the following nonlinear optimization problem.

$$\min_{U_N(t)} \sum_{k=0}^{N-1} \|x(k+1|t)\|_Q + \|\Delta u(k|t)\|_{R_1} + \|u(k|t)\|_{R_2} \quad (16a)$$

$$\text{subject to } \forall k = 0,\ 1, \cdots N-1 \quad x(k+1|t) = f_d\left(x(k|t), u(k|t)\right) \quad (16b)$$

$$x(0|t) = x(t) \quad (16c)$$

$$u(k|t) \in \bar{U}_k \quad (16d)$$

$$u(t) = u(0|t) \quad (16e)$$

where N is the number of steps of prediction horizon and $x(k|t)$ and $u(k|t)$ are the predicted state vector and the planned input vector after k time steps from time t. $\Delta u(k|t) = u(k|t) - u(k-1|t)$ is the control change rate. The control change rate can be described as: $\Delta u(k|t) = u(0|t) - u(k-1)$ at initial time step $k = 0$. And, $\bar{U}_k$ is the constrained input set, expressed as equality or inequality equations for the predicted states and the inputs. In addition, expression $\|x\|_Q$ means $x^T Q x$. The initial value of state prediction $x(0|t)$ is the state vector $x(t)$, estimated or measured online.

The cost function (16a) and constraint (16d) of the optimization problem are expressed non-linearly due to the non-linearity of the system model (16a). Therefore, the optimization problem finds a solution that minimizes the cost function while satisfying the constraints through nonlinear programming (NLP). By solving the optimization problem, we obtain the following optimized control sequence at time t:

$$U_N(t) = \{u(0|t), u(1|t), \ldots, u(N-1|t)\}. \quad (17)$$

The first element of $U_N(t)$, i.e., $u(0|t)$, is applied to the system at time t.

In this study, sequential quadratic programming (SQP) was used for NLP. SQP finds solutions to constrained nonlinear optimization problems by solving a sequence of quadratic programming (QP) sub-problems. In detail, the solution of each QP sub-problem is used to linearize and optimize the QP sub-problems in the next iteration step. By repeating this, the solution of nonlinear optimization converges. Through conversion to QP problems that can be calculated very efficiently using the active-set method, the amount of computation can be reduced compared to other NLP solvers(Tan et al., 2018; Zhu et al., 2016).

3.1. Cost function of NMPC

$$J = \sum_{k=0}^{N-1} q_{e_y}\left(e_y(k+1|t)\right)^2 + q_{e_\psi}\left(e_\psi(k+1|t)\right)^2 + r_{1,\delta}\left(\Delta\delta(k|t)\right)^2 + r_{1,a_x}\left(\Delta a_x(k|t)\right)^2 + r_{2,a_x}\left(a_x(k|t)\right)^2 \quad (18)$$

Equation (18) is the cost function of MPC of the proposed controller. For accurate path tracking, the

lateral offset error e_y and heading angle error e_ψ for the desired path should be minimized, and the cost function must therefore contain terms to reduce them. In addition, the proposed controller reduces excessive changes of the control inputs δ and a_x. Large change rates of the control inputs can cause jerk, which can lead to transient instability of the vehicle. Finally, a penalty for longitudinal acceleration is applied to prevent unnecessary braking. Braking more than necessary can infringe the driver's intentions, so it should be reduced. The cost function for this purpose is expressed for the current states, inputs and input rates. Overall, The weight matrices for the state vector and input vector are constructed as: $Q = diag(0,0,0,0,q_{e_y}, q_{e_\psi})$, $R_1 = diag(r_{1,\delta}, r_{1,a_x})$ and $R_2 = diag(0, r_{2,a_x})$ in the cost function of optimal problem (16).

3.2. Constraints of NMPC

The main purpose of this study is to prevent unstable behavior due to road friction limit during control time. For stable behavior, the controller must ensure that all tires generate a force below the road friction limit. Therefore, the proposed controller must satisfy the following conditions:

$$f_i(k|t) = \frac{1}{F_{z,i}(k|t)}\sqrt{\left(F_{x,i}(k|t)\right)^2 + \left(F_{y,i}(k|t)\right)^2} < \mu \quad \forall k = 0,\ 1, \cdots N-1, \forall i = fl, fr, rl, rr \tag{19}$$

where f_i is the normalized tire force of each wheel. Due to the above constraints, the control inputs are calculated taking into account the tire force during the prediction horizon. Therefore, it is possible to prepare in advance for future unstable behavior. It was assumed that the road friction limit is known through existing estimation methods (Khaleghian et al., 2017; Han et al., 2016; Han et al., 2017; Ray, 1997).

Also, to reduce excessive path tracking error, the constraints of lateral offset error and heading angle error are set as follows:

$$\begin{cases} e_y^l \le e_y(k+i|t) \le e_y^u \\ e_\psi^l \le e_\psi(k+i|t) \le e_\psi^u \end{cases} \quad \forall k = 0,\ 1, \cdots N-1. \tag{20}$$

Each tire force in constraint (19) is expressed as a function of state predictions and future inputs by (4)-(6) and (9), and constraints(20) are also expressed through state predictions. Since state predictions during the prediction horizon are determined by the current states $x(t)$ and the input sequence through system model (16b), constraints (19) and (20) are expressed as *x(t)* and u as follows :

$$h_{(k|t)}\big(x(t), u(k|t)\big) \le 0 \quad \forall k = 0,\ 1, \cdots N-1 \tag{21}$$

$$u(k|t) \in \bar{U}(k|t) \equiv \{u | h_{(k|t)}(x(t), u) \le 0\} \quad \forall k = 0,\ 1, \cdots N-1 \tag{22}$$

4. SIMULATION RESULTS

Simulations were conducted to verify the performance of the proposed controller. The simulations used Carsim, a high-order vehicle simulator, and the proposed controller was designed using Matlab Simulink. In the sub-sections, the comparison between the proposed and existing controllers and the performance of the proposed controller on various road surfaces are discussed. The control parameters utilized in the simulation are shown in Table 1; the desired path used in the simulations is shown in Figure 3.

Table 1. Control parameters.

Parameter	Value
T_s(s)	0.1
N	20
Q	diag(0, 0, 0, 0, 10, 10)
R_1	diag(30, 0.01)
R_2	diag(0, 0.0005)
e_y^l, e_y^u (m)	-0.2, 0.2
e_ψ^l, e_ψ^u (deg)	-5, 5

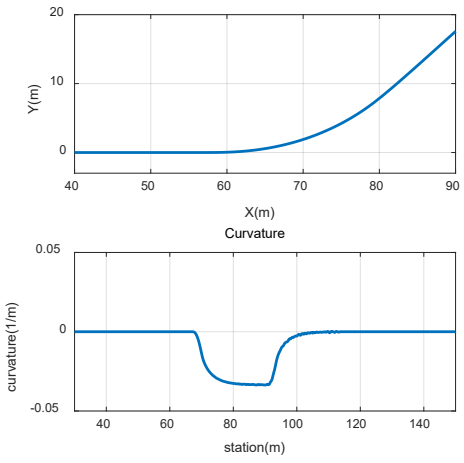

Figure 3. Desired path of simulation

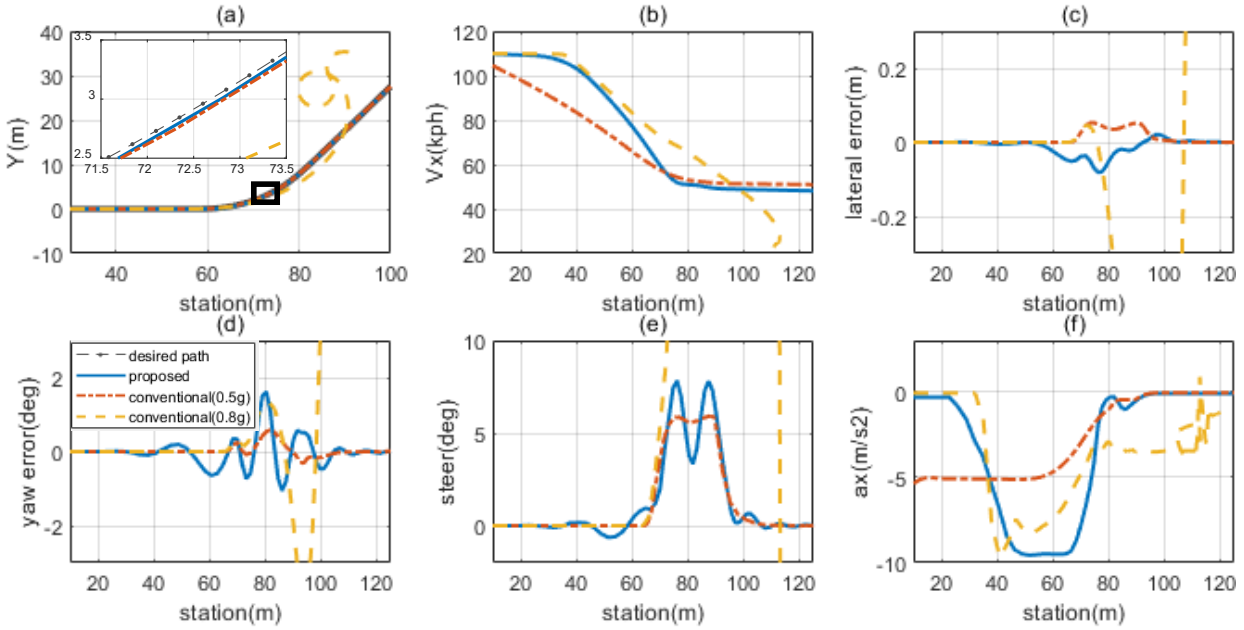

Figure 4. Vehicle behaviors and control inputs of proposed controller and the existing methods

4.1. Comparison with existing controller

The performance of the proposed controller was verified through comparisons on a high-mu road, i.e. $\mu = 1$. The conventional controllers designed for comparison performs speed control and lateral control separately. The desired velocity was calculated under the condition that the sum of the longitudinal and lateral accelerations

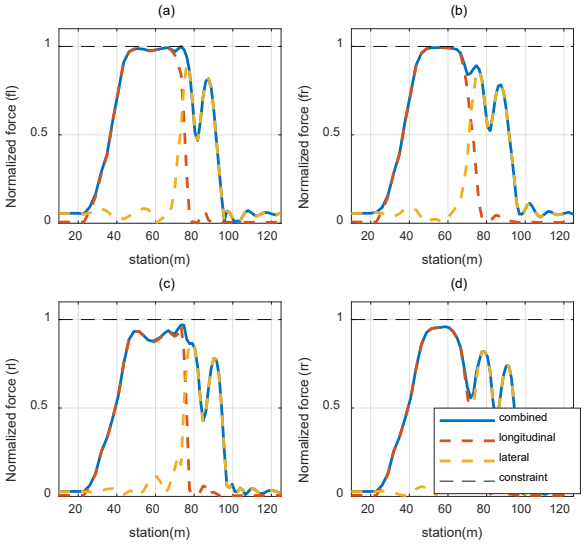

Figure 5. Normalized tire forces of proposed controller

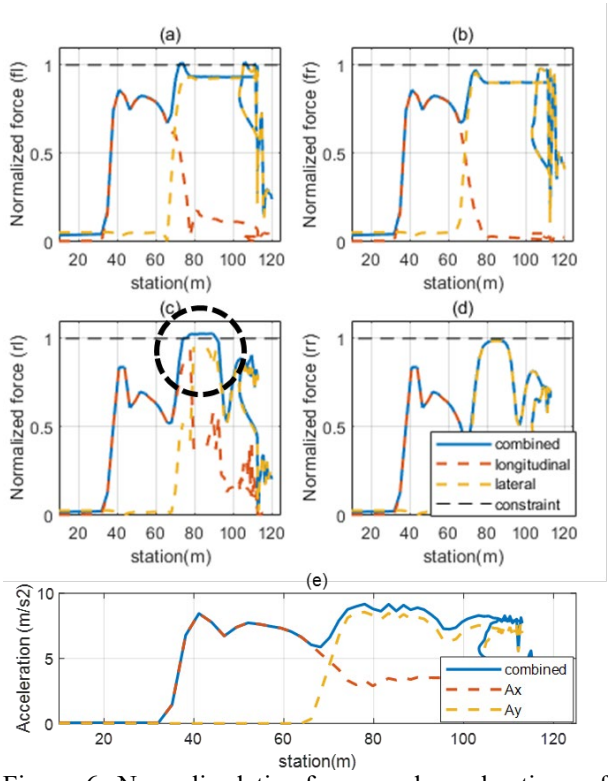

Figure 6. Normalized tire forces and accelerations of conventional controller (With 0.8g acceleration limit)

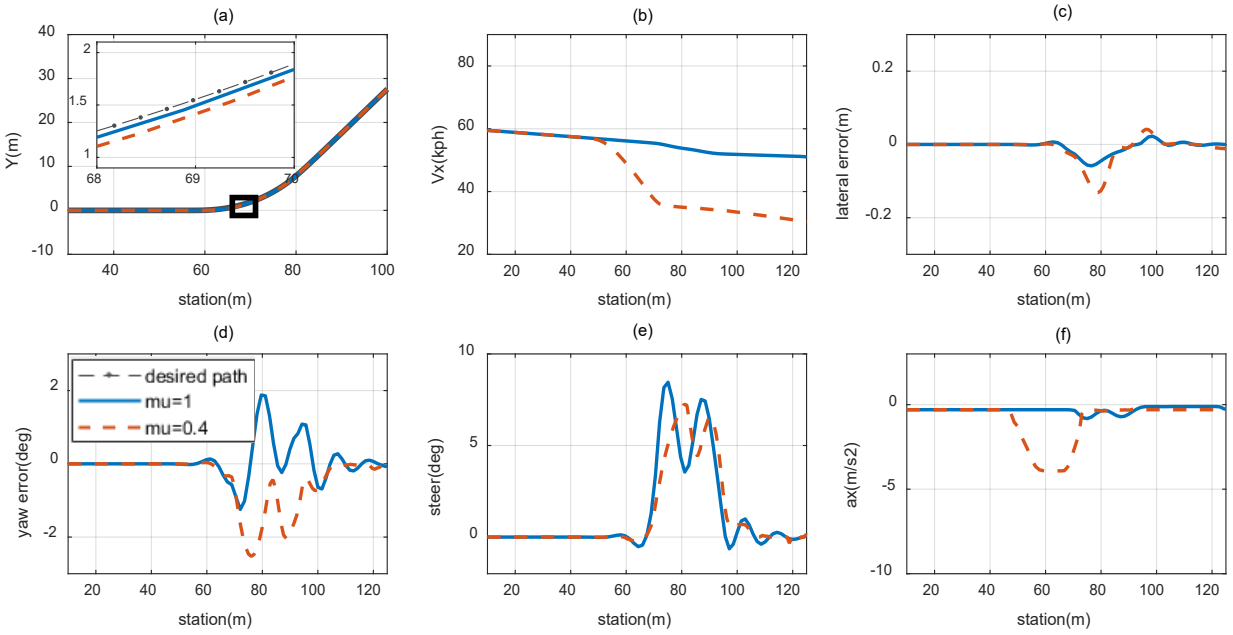

Figure 7. Vehicle behaviors and the control inputs of proposed controller on different friction surfaces (initial speed = 60 km/h)

occurs within a certain acceleration range, assuming the vehicle as a point mass. The lateral controller was implemented as NMPC with same prediction time.

The vehicle states and the applied inputs for each controller are shown in Figure 4, which shows that the proposed controller followed the path well through the tracking error expressed in Figure 4(c,d). The vehicle speed represented in Figure 4(b) shows that all results were controlled to decelerate before turning. In particular, the proposed controller was decelerated by the constraint (22) so that each normalized combined force represented in Figure 5 does not exceed the road surface friction limit. As a result, the force of each wheel was generated in a stable area, ensuring stable path tracking of vehicle.

However, in the case of conventional controllers performed through acceleration constraints, performance limitations exist at high initial speed situation. The results controlled with an acceleration constraint of 0.8 g show that the vehicle behaved unstable due to the tire friction limit. Although the combined acceleration shown in Figure 6(e) occurred less than the friction limit (i.e. $\sqrt{a_x^2 + a_y^2} < \mu g$), the vehicle became unstable as the tire force exceeds the road friction limit, as shown in Figure 6(c). It is due to the absence of consideration of condition of each wheel, such as the load transfer of vehicle, the difference in the slip angle of the front and rear tires, and the distribution of braking between the front and rear. Therefore, for stable path tracking, the acceleration constraint of the conventional controller must be set too conservatively. When controlled with a conservative acceleration constraint of 0.5g, the vehicle accurately tracked the desired path. However, compared to the proposed controller, braking control was performed in advance by about 20m or more. This means that the required preview distance is more than that of 20 m longer than the proposed controller. Therefore, stable control is not possible in situations in which the vehicle has a short preview distance or operates at a higher speed.

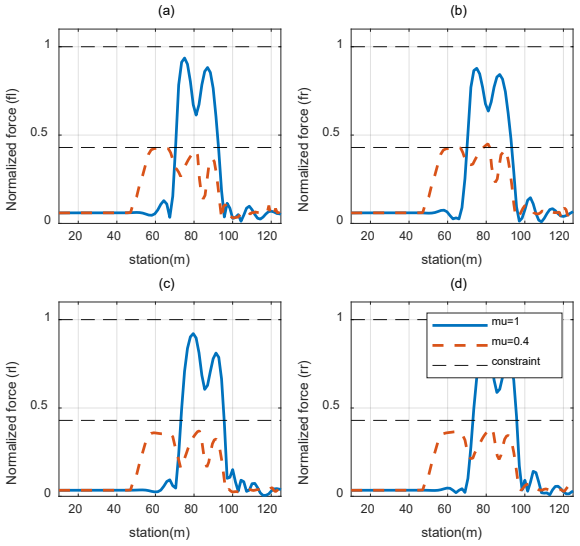

Figure 8. Normalized combined forces of each tire on dry and slippery road surfaces

4.2. Comparison of different friction surfaces

The performance of the proposed controller for different road surface conditions is shown in Figure 7. Simulations were conducted on dry($\mu = 1$) and slippery surfaces ($\mu = 0.4$) at the same initial speed (60 km/h). Using the constraint (19), the proposed controller caused the forces of each wheel to be less than the friction limit. Therefore, as shown in Figure 8, the normalized combined forces of each tire were under the road friction limit for each situation.

On the dry road surface, sufficient lateral force can be generated without deceleration, so only steering input was generated, without unnecessary braking input. As a result, the vehicle accurately followed the path at almost constant speed. A normalized force of up to 0.85 was generated. However, when entering a corner at the same speed on a slippery road surface, the vehicle was not able to generate as much lateral force as in the dry road condition. Therefore, the controller decelerated the vehicle in advance to satisfy constraint (19). The braking force at that time was also less than the road surface limit. As a result, the road friction limit constraint was satisfied, and the vehicle followed the desired path stably. Table 2 shows the control result values for each road surface condition.

Table 2. Simulation results of proposed controller on different friction surfaces (initial speed = 60 km/h)

Situation	Max $\lvert e_y \rvert$ (m)	v_x (km/h) at s=70m	Max f_i
μ =1	0.05	53.5	0.86
μ =0.4	0.13	37.6	0.40

4. CONCLUSION

This study proposes a path tracking controller that enables a vehicle to stably and accurately follow a desired path when it enters a curved path at high speed. The proposed controller performs not only steering control but also appropriate braking control before steering for high speeds that cannot be dealt with only by steering control. The integrated braking and steering controller was implemented through NMPC, which can respond to future vehicle conditions using nonlinear vehicle and tire models.

In particular, through the constraints of the NMPC, the proposed controller ensure that the tire forces of all wheels do not exceed the road friction limit. Therefore, all tires operated in a stable area and, through this, the vehicle also stably followed the desired path. In the simulation results using Carsim, it was verified that, compared the existing controller, the proposed controller can perform stable control with only a short preview distance. In addition, stable and accurate path tracking performance for various road surfaces was verified.

In the future work, for more reliable verification of the proposed controller performance, real vehicle verification will be performed. In addition, through the development of an adaptive algorithm using real time estimation of road friction, the performance and stability of the estimator-based control will be analyzed.

ACKNOWLEDGEMENT– This research was partly supported by the National Research Foundation of Korea(NRF) grant funded by the Korea government(MSIP) (No.2020R1A2B5B01001531); the BK21+ program through the NRF funded by the Ministry of Education of Korea; the Technology Innovation Program funded By the Ministry of Trade, Industry & Energy(MOTIE, Korea) (No.20010263); the National Research Foundation of Korea(NRF) grant funded by the Korea government(MSIP) (No.2020R1A2B5B01001531); and the Technology Innovation Program funded By the Ministry of Trade, Industry & Energy(MOTIE, Korea) (No.20014983).

REFERENCES

Doumiati M, Victorino AC, Charara A, et al. (2010) Onboard real-time estimation of vehicle lateral tire–road forces and sideslip angle. *IEEE/ASME Transactions on Mechatronics* 16(4): 601-614.

Gao Y, Lin T, Borrelli F, et al. (2010) Predictive control of autonomous ground vehicles with obstacle avoidance on slippery roads. *Dynamic systems and control conference.* 265-272.

Geronimo D, Lopez AM, Sappa AD, et al. (2009) Survey of pedestrian detection for advanced driver assistance systems. *IEEE transactions on pattern analysis and machine intelligence* 32(7): 1239-1258.

Gietelink O, Ploeg J, De Schutter B, et al. (2006) Development of advanced driver assistance systems with vehicle hardware-in-the-loop simulations. *Vehicle System Dynamics* 44(7): 569-590.

Gill PE and Wong E (2012) Sequential quadratic programming methods. *Mixed integer nonlinear programming*. Springer, pp.147-224.

Gray A, Ali M, Gao Y, et al. (2012) Integrated threat assessment and control design for roadway departure avoidance. *2012 15th International IEEE Conference on Intelligent Transportation Systems.* IEEE, 1714-1719.

Han K, Hwang Y, Lee E, et al. (2016) Robust estimation of maximum tire-road friction coefficient considering road surface

irregularity. *International journal of automotive technology* 17(3): 415-425.

Han K, Lee E, Choi M, et al. (2017) Adaptive Scheme for the Real-Time Estimation of Tire-Road Friction Coefficient and Vehicle Velocity. *IEEE/ASME Transactions on Mechatronics,* 22(4): 1508-1518.

Han K, Park G, Sankar GS, et al. (2020) Model predictive control framework for improving vehicle cornering performance using handling characteristics. *IEEE Transactions on Intelligent Transportation Systems* 22(5): 3014-3024.

Hu C, Wang R, Yan F, et al. (2015) Should the desired heading in path following of autonomous vehicles be the tangent direction of the desired path? *IEEE Transactions on Intelligent Transportation Systems* 16(6): 3084-3094.

Hu X, Chen L, Tang B, et al. (2018) Dynamic path planning for autonomous driving on various roads with avoidance of static and moving obstacles. *Mechanical Systems and Signal Processing* 100: 482-500.

Hwang Y and Choi SB (2018) Adaptive collision avoidance using road friction information. *IEEE Transactions on Intelligent Transportation Systems* 20(1): 348-361.

Ji J, Khajepour A, Melek WW, et al. (2016) Path planning and tracking for vehicle collision avoidance based on model predictive control with multiconstraints. *IEEE Transactions on Vehicular Technology* 66(2): 952-964.

Khaleghian S, Emami A and Taheri S (2017) A technical survey on tire-road friction estimation. *Friction* 5(2): 123-146.

Lim W, Lee S, Sunwoo M, et al. (2018) Hierarchical trajectory planning of an autonomous car based on the integration of a sampling and an optimization method. *IEEE Transactions on Intelligent Transportation Systems* 19(2): 613-626.

Liu J, Jayakumar P, Stein JL, et al. (2017) Combined speed and steering control in high-speed autonomous ground vehicles for obstacle avoidance using model predictive control. *IEEE Transactions on Vehicular Technology* 66(10): 8746-8763.

Liu J, Jayakumar P, Stein JL, et al. (2018) A nonlinear model predictive control formulation for obstacle avoidance in high-speed autonomous ground vehicles in unstructured environments. *Vehicle System Dynamics* 56(6): 853-882.

Paden B, Čáp M, Yong SZ, et al. (2016) A survey of motion planning and control techniques for self-driving urban vehicles. *IEEE Transactions on intelligent vehicles* 1(1): 33-55.

Park H-G, Ahn K-K, Park M-K, et al. (2018) Study on robust lateral controller for differential GPS-based autonomous vehicles. *International Journal of Precision Engineering and Manufacturing* 19(3): 367-376.

Pozna C, Troester F, Precup R-E, et al. (2009) On the design of an obstacle avoiding trajectory: Method and simulation. *Mathematics and Computers in Simulation* 79(7): 2211-2226.

Ray LR (1997) Nonlinear tire force estimation and road friction identification: Simulation and experiments. *Automatica* 33(10): 1819-1833.

Ren H, Chen S, Yang L, et al. (2020) Optimal path planning and speed control integration strategy for UGVs in static and dynamic environments. *IEEE Transactions on Vehicular Technology* 69(10): 10619-10629.

Rigatos G and Siano P (2014) An H-infinity feedback control approach to autonomous robot navigation. *IECON 2014-40th Annual Conference of the IEEE Industrial Electronics Society.* IEEE, 2689-2694.

Sazgar H, Azadi S, Kazemi R, et al. (2019) Integrated longitudinal and lateral guidance of vehicles in critical high speed manoeuvres. *Proceedings of the Institution of Mechanical Engineers, Part K: Journal of Multi-body Dynamics* 233(4): 994-1013.

Siampis E, Velenis E, Gariuolo S, et al. (2017) A real-time nonlinear model predictive control strategy for stabilization of an electric vehicle at the limits of handling. *IEEE Transactions on Control Systems Technology* 26(6): 1982-1994.

Simon D, Löfberg J and Glad T (2013) Nonlinear model predictive control using feedback linearization and local inner convex constraint approximations. *2013 European Control Conference (ECC).* IEEE, 2056-2061.

Svendenius J, Gäfvert M, Bruzelius F, et al. (2009) Experimental validation of the brush tire model. *Tire Science and Technology* 37(2): 122-137.

Tan Q, Dai P, Zhang Z, et al. (2018) MPC and PSO based control methodology for path tracking of 4WS4WD vehicles. *Applied Sciences* 8(6): 1000.

Wang C, Sun Q, Guo Y, et al. (2019) Improving the user acceptability of advanced driver assistance systems based on different driving styles: A case study of lane change warning systems. *IEEE Transactions on Intelligent Transportation Systems* 21(10): 4196-4208.

Wurts J, Stein JL and Ersal T (2020) Collision imminent steering at high speed using nonlinear model predictive control. *IEEE Transactions on Vehicular Technology* 69(8): 8278-8289.

Xu S and Peng H (2019) Design, analysis, and experiments of preview path tracking control for autonomous vehicles. *IEEE Transactions on Intelligent Transportation Systems* 21(1): 48-58.

Zakaria MA, Zamzuri H, Mamat R, et al. (2014) Dynamic curvature path tracking control for autonomous vehicle: Experimental results. *2014 International Conference on Connected Vehicles and Expo (ICCVE).* IEEE, 264-269.

Zhu Q, Onori S and Prucka R (2016) Nonlinear economic model predictive control for SI engines based on sequential quadratic programming. *2016 American Control Conference (ACC).* IEEE, 1802-1807.